Chemical Science

ROYAL SOCIETY OF CHEMISTRY

EDGE ARTICLE



Cite this: *Chem. Sci.*, 2020, **11**, 6510

All publication charges for this article have been paid for by the Royal Society of Chemistry

# A regioselectively 1,1′,3,3′-tetrazincated ferrocene complex displaying core and peripheral reactivity†

Gordon W. Honeyman,[a] David R. Armstrong,[a] William Clegg,[b] Eva Hevia,‡[a] Alan R. Kennedy,[a] Ross McLellan,[a] Samantha A. Orr,§[a] John A. Parkinson,[a] Donna L. Ramsay,[a] Stuart D. Robertson,*[a] Stephen Towie[a] and Robert E. Mulvey*[a]

Regioselective 1,1′,3,3′-tetrazincation [C–H to C–Zn(*t*Bu)] of ferrocene has been achieved by reaction of a fourfold excess of di-*t*-butylzinc ($t$Bu$_2$Zn) with sodium 2,2,6,6-tetramethylpiperidide (NaTMP) in hexane solution manifested in the trimetallic iron–sodium–zinc complex [Na$_4$(TMP)$_4$Zn$_4$(*t*Bu)$_4${(C$_5$H$_3$)$_2$Fe}], **1**. X-ray crystallographic studies supported by DFT modelling reveal the structure to be an open inverse crown in which two [Na(TMP)Zn(*t*Bu)Na(TMP)Zn(*t*Bu)]$^{2+}$ cationic units surround a {(C$_5$H$_3$)$_2$Fe}$^{4-}$ tetraanion. Detailed C$_6$D$_6$ NMR studies have assigned the plethora of $^1$H and $^{13}$C chemical shifts of this complex. It exists in a major form in which capping and bridging TMP groups interchange, as well as a minor form that appears to be an intermediate in this complicated exchange phenomenon. Investigation of **1** has uncovered two distinct reactivities. Two of its peripheral *t*-butyl carbanions formally deprotonate toluene at the lateral methyl group to generate benzyl ligands that replace these carbanions in [Na$_4$(TMP)$_4$Zn$_4$(*t*Bu)$_2$(CH$_2$Ph)$_2${(C$_5$H$_3$)$_2$Fe}], **2**, which retains its tetrazincated ferrocenyl core. Benzyl-Na π-arene interactions are a notable feature of **2**. In contrast, reaction with pyridine affords the crystalline product {[Na·4py][Zn(py*)$_2$(*t*Bu)·py]}$_\infty$, **3**, where py is neutral pyridine (C$_5$H$_5$N) and py* is the anion (4-C$_5$H$_4$N), a rare example of pyridine deprotonated/metallated at the 4-position. This ferrocene-free complex appears to be a product of core reactivity in that the core-positioned ferrocenyl anions of **1**, in company with TMP anions, have formally deprotonated the heterocycle.

Received 18th March 2020
Accepted 26th March 2020

DOI: 10.1039/d0sc01612h

rsc.li/chemical-science

## Introduction

Second generation metallation, where the Brønsted base is a multicomponent compound or mixture, instead of a single organolithium reagent [1] or lithium amide reagent[2] as in the first generation types, is now well established.[3] In terms of synthetic utility, Knochel's salt-activated[4] metal amide reagents have proved most popular, typified by magnesium complexes such as (TMP)MgCl·LiCl[5] and zinc complexes such as (TMP)$_2$-Zn·2MgCl$_2$·2LiCl,[6] though many others have also been applied successfully in deprotonation reactions.[7] The vast majority of these reactions have involved monodeprotonations of organic substrates, while di-deprotonative metallations are usually unwanted side reactions, generally indirectly identified through detection of difunctionalised products following electrophilic interception protocols.[8] Much less developed are poly-metallation reactions, where di- or higher order-deprotonation is a deliberate aim. A special category of metallation called template magnesiation is an exception.[9] Here, the degree as well as the regioselectivity of deprotonation are dictated mainly by the preformed structure of the second-generation base. For example, the 24-atom template ring structure of hexameric [{KMg(TMP)$_2$(*n*Bu)}$_6$] can deprotonate six naphthalene molecules with its six Mg-fixed butyl bases, while retaining the [(KNMgN)$_6$] ring in the product [{KMg(TMP)$_2$(2-C$_{10}$H$_7$)}$_6$].[10] The related sodium template [Na$_4$Mg$_2$(TMP)$_6$(*n*Bu)$_2$] with its 12-atom (NaNMgNNaN)$_2$ template ring di-deprotonates *para*-terphenyl on one terminal Ph ring to generate [Na$_4$Mg$_2$(TMP)$_6$(3,5-*para*-terphenyl-di-ide)], or four times (twice on each terminal Ph ring) to afford [{Na$_4$Mg$_2$(TMP)$_6$}$_2$(3,3″,5,5″-*para*-terphenyl-tetra-ide)].[9a]

Ferrocenes and their functionalized derivatives are important molecules in a remarkably wide variety of fields such as in materials, as pharmaceuticals and as components of chiral and

[a]*WestCHEM, Department of Pure & Applied Chemistry, University of Strathclyde, Glasgow, G1 1XL, UK. E-mail: r.e.mulvey@strath.ac.uk; stuart.d.robertson@strath.ac.uk*

[b]*Chemistry, School of Natural and Environmental Sciences, Newcastle University, Newcastle upon Tyne, NE1 7RU, UK*

† Electronic supplementary information (ESI) available. CCDC 1972641–1972644. For ESI and crystallographic data in CIF or other electronic format see DOI: 10.1039/d0sc01612h

‡ Current address: Department für Chemie und Biochemie, Universität Bern, CH3012, Bern, Switzerland.

§ Current address: School of Chemistry, Monash University, Clayton, Melbourne, VIC 3800, Australia.

achiral ligands for catalysis.[11] Previously, such fourfold deprotonation was accomplished with ferrocene in $[Na_4Mg_4(NiPr_2)_8\{Fe(C_5H_3)_2\}]$, using a sodium magnesium diisopropylamide base,[12] while recently a first-generation potassium alkoxy neopentyl complex has also achieved tetradeprotonation though the ferrocenylpotassium product could not be characterised.[13] Ferrocene is typically more susceptible to mono- or dideprotonation (one deprotonation per ring),[14] meaning controlled tetradeprotonation would provide access to a potentially useful synthetic intermediate.[15] Since zinc is a key component of many synergistic compounds[16] and offers more onward functionalization opportunities than magnesium (*e.g.*, through Negishi cross-coupling processes),[17] it would be useful to develop a complementary zinc chemistry of this controlled higher order deprotonation. This work sets out on this path, reporting the first reaction exhibiting four C–H to C–Zn exchanges in an open inverse crown product[15a,18] the openness of which enables peripheral and core reactivities not observed previously in inverse crown chemistry.

## Results and discussion

### Synthesis and solid-state studies of tetrametallated complex 1

In earlier work we showed it was possible to effect mono- and dizincation of ferrocene using the appropriate amount of TMP-zincate reagent TMEDA·Na(μ-TMP)(μ-*t*Bu)Zn*t*Bu,[19] with crystal structures of TMEDA·Na(μ-TMP)[μ-$(C_5H_4)$Fe$(C_5H_5)$]Zn*t*Bu (**A**) and [TMEDA·Na(μ-TMP)Zn*t*Bu]$_2(C_5H_4)_2$Fe (**B**) being obtained in each case though NMR studies established that stoichiometric control was not perfect with each solution containing traces of the incorrect stoichiometric product. A hint that higher order zincation might be realised came from isolation of a poorly soluble red powder on treating ferrocene with four equivalents of the base mixture in the absence of Lewis donating TMEDA.[20] Different isomers of a putative tetrazincation product were implicated on the sole evidence of a routine $^1$H NMR spectrum, forming the starting point for the present study. Following many attempts, we have managed to coax red crystals from this reaction (Scheme 1) and analysed them by X-ray crystallography.

Frustratingly, these crystals and different batches from several reproducible reactions proved highly disordered. There are 3 crystallographically independent molecules in the structure, one of which is completely disordered around a centre of symmetry and one molecule has a disordered *t*Bu group. However, one molecule is well ordered (Fig. 1) and so it is reasonable to conclude that the bulk of the product is the expected tetrazincated ferrocene $[Na_4(TMP)_4Zn_4(tBu)_4\{(C_5H_3)_2Fe\}]$, **1**. The four zinc atoms occupy the 1,1′,3,3′ sites on the ferrocene scaffold commensurate with tetradeprotonation

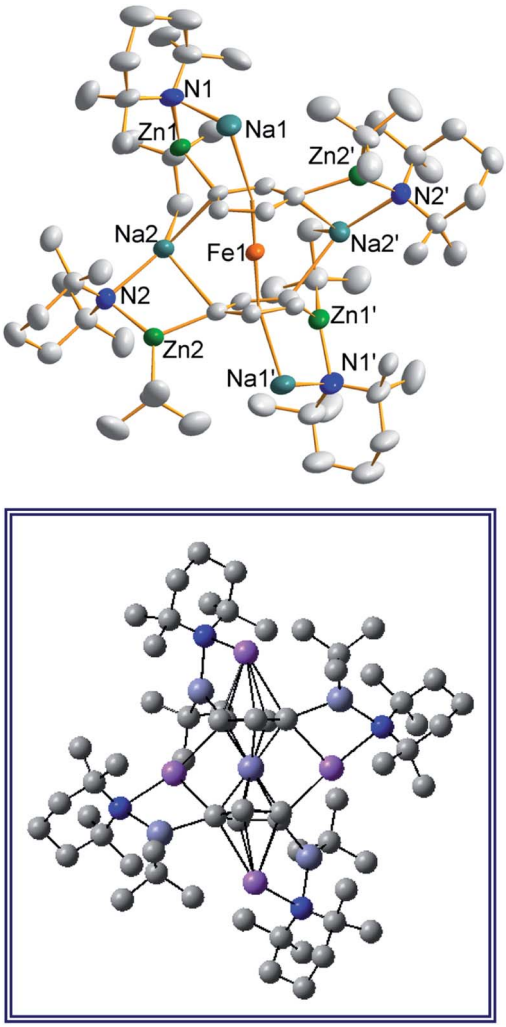


Fig. 1 Molecular structure of one independent molecule of the tetrazincated ferrocene $[Na_4(TMP)_4Zn_4(tBu)_4\{(C_5H_3)_2Fe\}]$ (**1**, top) and DFT optimised structure ($\mathbf{1}_{calc}$, bottom). Ellipsoids are shown at 50% probability and all hydrogen atoms have been removed for clarity. Selected bond lengths (Å) and angles (°) for $\mathbf{1}_{calc}$: Na1–N1, 2.374; Zn1–N1, 2.046; Zn1–$C_{Fc}$, 2.120; Zn1–$C_{tBu}$, 2.045; Na2–$C_{tBu}$, 2.883; Na2–N2, 2.414; Na2, $C_{Fc}$, 2.624, 2.651; Zn2–$C_{Fc}$, 2.085; Zn2–N2, 2.041; Zn2–$C_{tBu}$, 2.061; Na1–$C_{tBu}$, 2.922; Na1–N1–Zn1, 92.1; Na1–$C_{Fc}$–Zn1, 83.1; N1–Zn1–$C_{Fc}$, 102.7; N1–Na1–$C_{Fc}$, 80.5; Na2–N2–Zn2, 83.9; Na2–$C_{Fc}$–Zn2, 77.3; N2–Zn2–$C_{Fc}$, 112.6; N2–Na2–$C_{Fc}$, 85.2; $C_{Fc}$–Na2–$C_{Fc}$, 87.0.

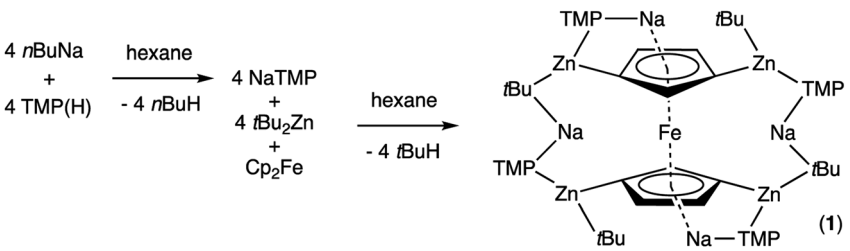


Scheme 1 Synthetic protocol for accessing the tetrazincated ferrocene complex.

having occurred. Two zinc atoms bridge through a TMP ligand to the sodium atoms capping the $C_5H_3$ rings, while the other two zinc atoms each bridge through a TMP ligand to the centrally disposed sodium centres positioned either side of the iron. The remaining coordination site on each zinc atom is filled by an alkyl ligand. Consequently, with the two zinc atoms bound to each Cp ring being inequivalent, this can be considered as a planar chiral complex (see NMR section for further discussion). In earlier work the magnesiated ferrocene $[Na_4Mg_4(NiPr_2)_8\{Fe(C_5H_3)_2\}]$ has been interpreted as an inverse crown[10,21] comprising a 16-membered $[(NaNMgN)_4]$ cationic (4+ charged) ring that hosts a $[Fe(C_5H_3)_2\}]$ (4− charged) guest. Though related, **1** has structural features that sets it apart from this magnesiated structure in having a heteroleptic ligand set of alternating amido and alkyl groups and a less complete (or totally open) $[\{Na(TMP)Zn(alkyl)\}_4]^{4+}$ unit in the cationic moiety surrounding the $[(C_5H_3)_2Fe]^{4-}$ core. A DFT optimisation $\mathbf{1_{calc}}$ (Fig. 1 inset, with enforced $C_2$ symmetry corresponding to the symmetry of the experimental structure) starting from the experimental X-ray established coordinates of **1** predicts the cationic moiety in this structure is totally open having terminal *t*Bu ligands bound to Zn2. This is demonstrated by the closest methyl group of this terminal *t*Bu group to the adjacent sodium which is almost 3 Å away (calculated distance is 2.922 Å) compared with the bridging *t*Bu group of TMEDA·Na(μ-TMP)(μ-*t*Bu)Zn*t*Bu which has significantly shorter distances of 2.750(10) Å [22] and 2.818(13)/2.837(15) Å for the *t*Bu groups bridging sodium and zinc in complex **3** (*vide infra*) and 2.883 Å for the corresponding Na2–$C_{tBu}$ distance in this complex. Previously studied tetramagnesiated metallocenes (Ru and Os examples, besides the aforementioned Fe example) have been analysed *via* DFT calculations from which it was concluded that two isomeric forms (assigned *Z* and *W* for $C_i$ and $C_2$ symmetrical variants respectively) are possible with the *Z* form (characterized by having a symmetry imposed linear Na···Fe···Na unit) being the prevalent one.[23] In this case the solid-state structure appears to adopt the W form (Fig. 2) as evidenced by the bent Na···Fe···Na unit. This variation is perhaps unsurprising since the guest molecule (tetradeprotonated ferrocene) is identical but the inverse crown host ring (assuming a long-distance contact between Na and the methyl group of the *t*Bu ligand) surrounding it formally contains 20 atoms as opposed to 16 and so a deformation of this ring in the case of the *W* isomer is plausible.

Also revealing is the space-filling model of $\mathbf{1_{calc}}$ (Fig. 3) in showing that Na1 is much less well protected in this arrangement making it more susceptible to onward reactivity than the other sodium environment between the planes of the cyclopentadienyl rings, which is clearly more hidden and thus less available to coordinate potential substrates.

### Solution state study of 1

Solution phase NMR analysis of complex **1** solubilized in $C_6D_6$ revealed dynamic characteristics not considered in the solid-state study. These characteristics were revealed following extensive and detailed $^1$H and $^{13}$C NMR data analysis using both 2D [$^1$H, $^1$H] and 2D [$^1$H, $^{13}$C] correlation data sets. Full details of the deductive reasoning behind the data interpretation are provided in the ESI (Fig. S1–S10 and Tables S1–S3†). Basic evidence existed for the presence in solution of a minor species alongside the major form. Following data analysis, it was clear that the major form of the complex in solution reflected the crystal structure (*W*-isomer) form. No definite conclusion could be drawn regarding the structure of the minor species although it can tenuously be assigned to a *Z*-isomeric intermediate. The distinction of NMR resonances for Cp ring protons arising from major and minor forms of the complex was supported by 2D [$^1$H, $^1$H] EXSY NMR data for the sample studied at 298 K. This revealed clear evidence of chemical exchange between major

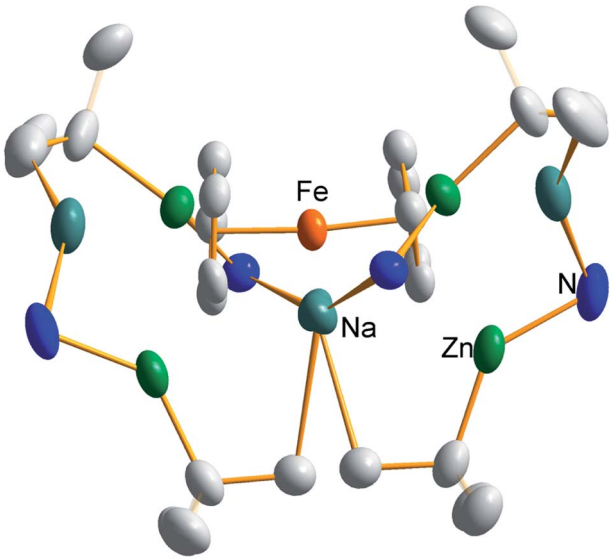


Fig. 2 Alternative perspective looking through the Na···Na axis, emphasising the "*W*-isomeric" form of complex **1**.

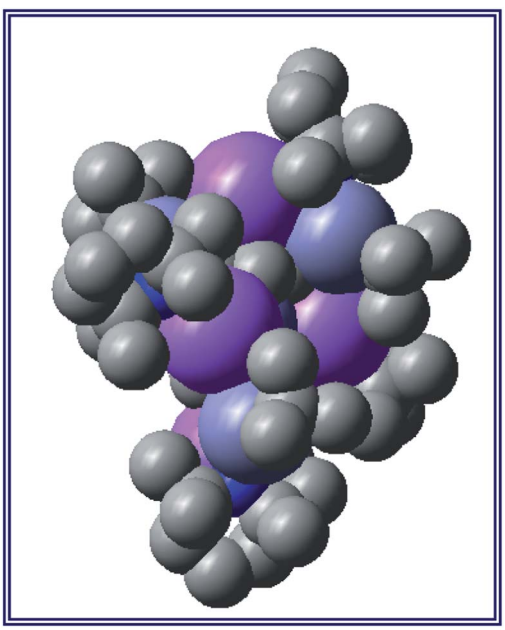

Fig. 3 Space-filling model of complex $\mathbf{1_{calc}}$.

and minor forms. Deeper investigation of this phenomenon revealed a further, concerted, intramolecular structural rearrangement of the major form of the complex. We speculate that the minor form could be present for one of two reasons or both. The minor (speculatively 'open') form of the complex could be an 'active' structure which allows for bond making and breaking to occur at the Cp ring. Alternatively, the minor form of the complex could be an 'open' intermediate species, which exists during rearrangement of the major form of the complex (Fig. 4).

The minor species could also be present serving both purposes or neither. It was not possible to define a structure for the minor species but we were intrigued by the observed changes in chemical shifts revealed through analysis of the chemical exchange process. Particularly noteworthy were the large changes in chemical shifts for $TMP_bMe20$ and $TMP_bMe22$ ($\Delta\delta^1H$ = 0.788 ppm and 0.612 ppm to lower chemical shift respectively; see Fig. 4 for numbering system) whilst deshielding occurred for $TMP_cMe6$ and $TMP_cMe7$ ($\Delta\delta^1H$ = 0.476 ppm and 0.308 ppm to higher chemical shift respectively; note b = bridging and c = capping). These changes suggest significant rearrangement of the structure in which the $TMP_b$ rings stack above the Cp rings and the $TMP_c$ rings assemble in a planar fashion adjacent to the Cp rings. This is consistent with chemical exchange-related EXSY NMR cross-peaks assigned to the intramolecular rearrangement of the major form of the complex. This reveals that capping and bridging groups interchange. Supporting evidence for this comes *via* chemical exchange cross-peaks between CpH27 and CpH28 resonances. This is only possible through intramolecular rearrangement of the major form to an identical but mirror image form. We therefore speculate that the minor form of the complex exists as a unique species, present with a relatively long lifetime (and therefore observable by NMR) as a half-way transition point between the oppositely handed major forms of the complex. Such an explanation may help to uncover how the chemistry of this complex is performed in the solution phase. A full analysis of the exchange rate characteristics, based on inspection of the Cp proton resonances, were derived through this interpretation and are reported in the ESI.† Overall, we conclude that an "opening" mechanism exists for this complex in solution in which the TMP and *t*Bu groups relocate into quite different magnetic environments, after which the structure "closes" into either the same handed or the oppositely handed major form of the complex.

### Reactivity of complex 1

Quenching of complex **1** with $D_2O$ resulted in the formation of $D_4$-Fc as evidenced by a GC-MS analysis with the predominant peak occurring at *m*/*z* 190.1, (Fig. S11†) consistent with tetra-deuterated $Fe(C_5H_3D_2)_2$. On comparing with the predicted mass spectrum (Fig. S12†), it appears that a small amount of tri-deuterated ferrocene is also present due to the presence of small peaks at 189 and 187, which should be absent for pure tetra-deuterated ferrocene. That notwithstanding, it is clear that $D_4$-Fc is the major product. Other peaks observed include $C_5H_3D_2$ at *m*/*z* 67.2 and $Fe(C_5H_3D_2)$ at 123.0.

Further investigation of the tetrazincated ferrocenyl complex **1** revealed novel and unexpected onward reactivity in its reactions with aromatic ring compounds. With toluene, **1** reacts through its peripheral alkyl ligands to deprotonate the lateral methyl arm and form the bis-benzyl derivative $[Na_4(TMP)_4Zn_4(tBu)_2(CH_2Ph)_2\{(C_5H_3)_2Fe\}]$ (complex **2**, Scheme 2) in which the tetrasodium tetrazincated ferrocenyl scaffold remains intact. Interestingly, only two of the four *t*butyl arms of **1** react, specifically the zinc-bonded terminal ones located above and below the plane of the cyclopentadienyl rings, with the other two (more protected) bridging *t*butyl groups remaining unreacted. To the best of our knowledge the transformation of complex **1** into complex **2** is the first example of peripheral

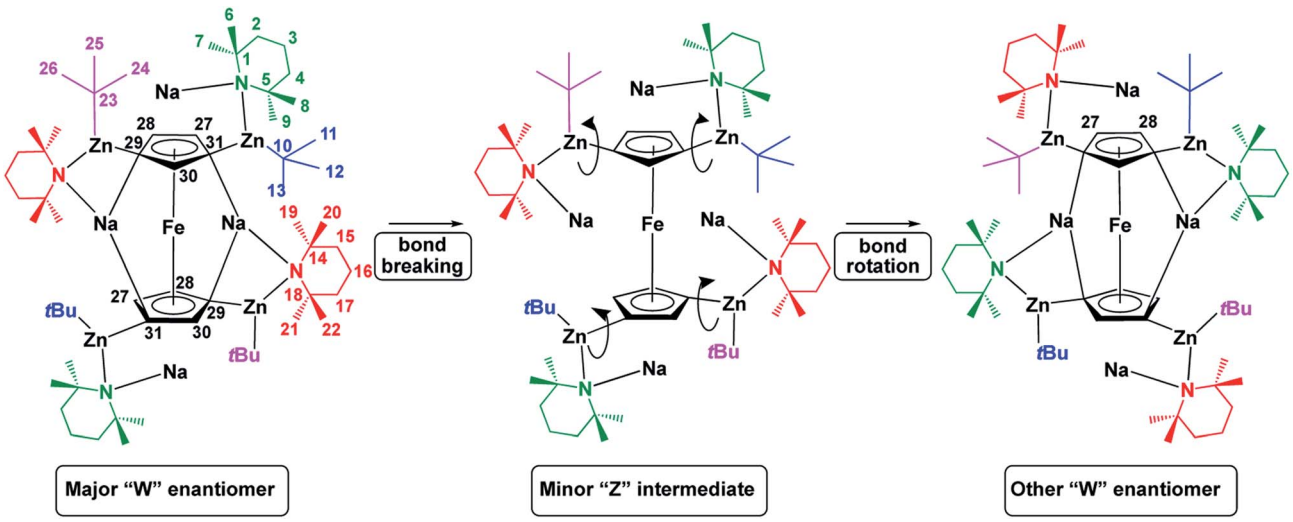


Fig. 4 Potential interconversion of major isomer of **1** to its other enantiomer *via* a minor intermediate, with proton numbering system used in discussion shown for clarity. Colour coding is used to clarify movement of ligands upon rearrangement and not to specify whether a ligand is bridging/capping for example.

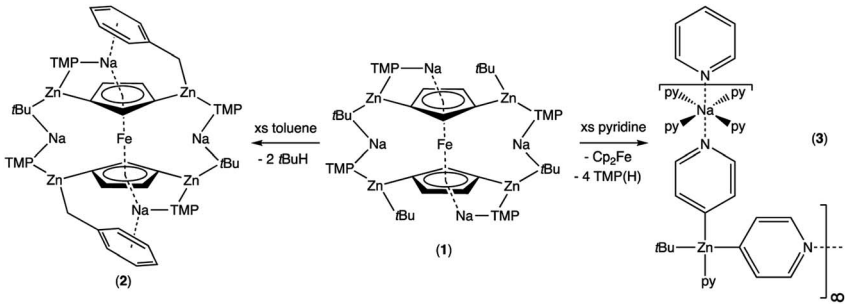


Scheme 2 Divergent reactivity of complex **1** with toluene and pyridine.

reactivity of an inverse crown complex, whereby an anionic component of the cationic $\{Na_4(TMP)_4Zn_4(tBu)_4\}^{4+}$ unit engages in a deprotonation reaction. Interestingly, however, the location of toluene deprotonation is at the most thermodynamically acidic position[24] and is thus in contrast to the synergistically-operative reactivity of TMEDA·Na(μ-TMP)(μ-*t*Bu)Zn*t*Bu, which preferentially deprotonates toluene at a ring position *via* a stepwise TMP deprotonation followed by a *t*-butyl deprotonation of TMP(H) releasing butane and reforming TMP to generate TMEDA·Na(μ-TMP)(μ-$C_6H_4$Me)Zn*t*Bu.[25] In gross features the structural motif of **2** is similar to that of **1** (Fig. 5, see Table 1 for selected bond lengths and angles). A tetrazincated core is encapsulated by a heteroleptic inverse crown which is now closed due to the bridging nature of the newly formed benzyl anions which, in turn, coordinate the zinc in a σ-fashion through the $CH_2$ anion and the sodium in more of a π-fashion through the aromatic ring.[26] This σ–π distinction has been observed in other mixed alkali metal–zinc complexes.[26b,27]

For completeness, we also carried out a DFT optimisation giving $\mathbf{2_{calc}}$, again starting from the experimental X-ray established coordinates of **2**. The $\Delta E$ of the reaction of complex **1** with two equivalents of toluene to yield complex **2** and two molar equivalents of isobutane was calculated as being −35.40 kcal mol$^{-1}$. The $^1$H NMR spectrum of complex **2** (Fig. S13†) was, as that of complex **1**, highly complicated within the aliphatic region. However, the 3.5–4.5 ppm region was similar to that of complex **1**, showing two sets of equal integration singlets indicative of a symmetrical 1,1′,3,3′-tetrametallated ferrocene.

Treating complex **1** with neat pyridine resulted in considerably divergent reactivity from that with toluene. The product complex **3** was shown by X-ray crystallography (Fig. 6) to be a chain polymer of formula $\{[Na\cdot 4py][Zn(py^*)_2(tBu)\cdot py]\}_\infty$, where py is solvating pyridine ($C_5H_5N$) and py* is an anionic derivative of pyridine formed through deprotonation of the heterocycle at the 4-position (4-$C_5H_4N$). The structure can be considered an ate arrangement in that the sodium centre is formally positive (surrounded by six solvating Lewis-donor pyridyl N-atoms in an approximate octahedral arrangement); while the monoanionic zinc moiety adopts a tetrahedral zincate structure consisting of a *t*butyl anion, two pyridyl C-anions and a neutral pyridine molecule. The polymer propagates *via* a pair of pyridyl anions acting as a N,C ditopic linker between sodium (N bound) and zinc (C bound). With respect to sodium, these linking molecules are *trans*-disposed, effecting a near linear unit to the polymer while the near tetrahedral nature of the zinc [C23–Zn–C28 bond angle = 114.28(18)°] enforces the zig–zagging conformation (Fig. 7). Each polymeric chain propagates

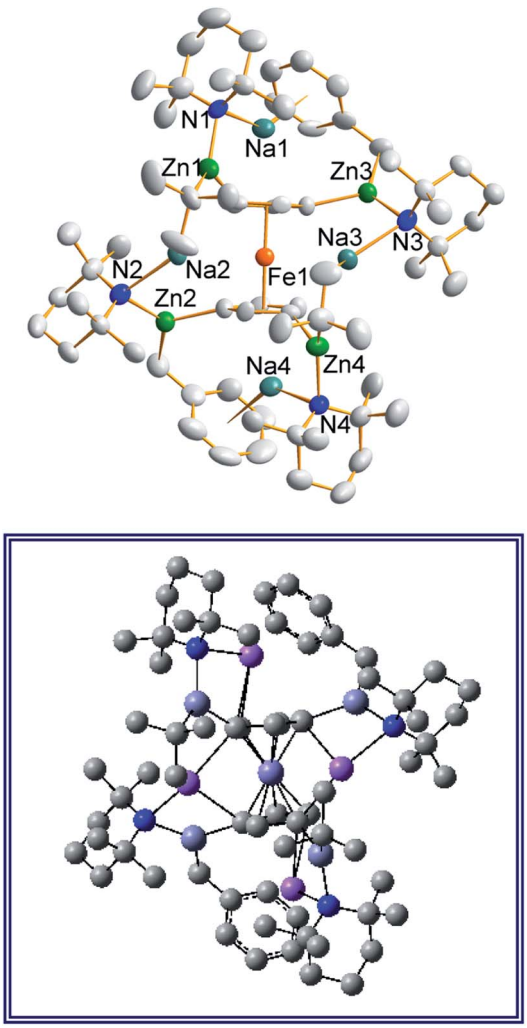


Fig. 5 Molecular structure of the tetrazincated ferrocene complex $[Na_4(TMP)_4Zn_4(tBu)_2(CH_2Ph)_2\{(C_5H_3)_2Fe\}]$ (**2**, top) and DFT optimised structure ($\mathbf{2_{calc}}$, bottom). Ellipsoids are shown at 50% probability and all hydrogen atoms have been removed for clarity.

 

Table 1 Selected bond parameters (Å and °) of complex **2** (values in bold represent relevant calculated parameters in $\mathbf{2}_{calc}$)

| | M(1) | M(2) | M(3) | M(4) |
|---|---|---|---|---|
| Zn–$C_{Fc}$ | 2.087(10), **2.108** | 2.022(10), **2.038** | 2.016(10), **2.037** | 2.076(10), **2.107** |
| Zn–$C_{Bz}$ | — | 2.031(11), **2.057** | 2.049(10), **2.058** | — |
| Zn–$C_{tBu}$ | 2.072(12) | — | — | 2.059(12) |
| Zn–$N_{TMP}$ | 2.017(9), **2.040** | 2.013(9), **2.027** | 2.018(8), **2.027** | 2.020(9), **2.040** |
| Na–$N_{TMP}$ | 2.447(9), **2.467** | 2.386(10), **2.422** | 2.355(10), **2.424** | 2.477(9), **2.463** |
| Na–$C_{Fc}$ | 2.456(4)[a] | 2.707(11), 2.562(12), **2.707**, **2.597** | 2.698(10), 2.562(11), **2.705**, **2.604** | 2.498(4)[a] |
| Na–$C_{Bz}$ | 2.711(3)[a] | — | — | 2.686(5)[a] |
| Na–$C_{tBu}$ | — | 2.847(15)[b] | 2.812(13)[b] | — |
| C–Zn–$C_{Fc}$ | 120.2(5) | 116.6(5) | 116.8(4) | 116.8(4) |
| C–Zn–$N_{TMP}$ | 134.2(4) | 127.5(4) | 127.8(4) | 135.1(4) |
| $C_{Fc}$–Zn–$N_{TMP}$ | 103.8(4), **103.4** | 115.8(4), **118.0** | 114.8(4), **117.9** | 104.1(4), **103.3** |
| $C_{Bz}$–Na–$N_{TMP}$ | 141.8(2)[c] | — | — | 139.6(3)[c] |
| $C_{Bz}$–Na–$C_{Fc}$ | 112.2(1)[c,d] | — | — | 114.5(2)[c,d] |
| $C_{Fc}$–Na–$N_{TMP}$ | 106.0(3)[d] | — | — | 105.8(2)[d] |
| $C_{Fc}$–Na–$C_{Fc}$ | — | 86.4(3), **86.5** | 85.9(3), **86.6** | — |
| $C_{Fc}$–Na–$N_{TMP}$ | — | 152.1(3), 84.0(3), **85.4** | 149.1(3), 84.3(3), **85.3** | — |
| Na–$N_{TMP}$–Zn | 92.6(3), **93.3** | 83.5(3), **81.4** | 84.0(3), **81.5** | 91.0(3), **93.2** |
| Na–$C_{Fc}$–Zn | 84.9(4), **84.8** | 75.4(3), **74.4** | 75.6(3), **74.6** | 84.6(3), **84.6** |

[a] Distance to benzyl is to centroid of aromatic ring. [b] Distance is to closest methyl carbon. [c] Angle at benzyl is from centroid of aromatic ring. [d] Angle at ferrocene is from centroid of Cp ring.

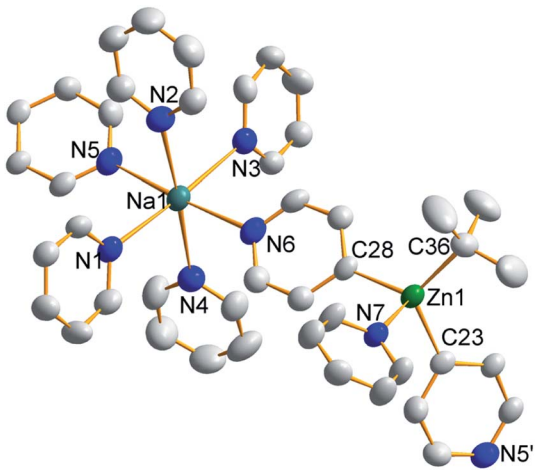


Fig. 6 Structure emphasising the asymmetric unit of sodium zincate $\{[Na\cdot 4py][Zn(py^*)_2(tBu)\cdot py]\}_\infty$ (**3**). Ellipsoids are shown at 50% probability and all hydrogen atoms have been removed for clarity. Selected bond lengths (Å) and angles (°): Na1–N1, 2.512(4); Na1–N2, 2.586(5); Na1–N3, 2.533(5); Na1–N4, 2.600(5); Na1–N5, 2.583(5); Na1–N6, 2.548(4); Zn1–N7, 2.254(3); Zn1–C23, 2.057(5); Zn1–C28, 2.061(4); Zn1–C36, 2.049(4); N1–Na1–N2, 89.52(15); N1–Na1–N3, 176.30(15); N1–Na1–N4, 88.09(15); N1–Na1–N5, 91.30(15); N1–Na1–N6, 93.76(13); N2–Na1–N3, 87.09(15); N2–Na1–N4, 177.04(16); N2–Na1–N5, 88.38(14); N2–Na1–N6, 92.62(14); N3–Na1–N4, 95.25(15); N3–Na1–N5, 87.13(15); N3–Na1–N6, 87.87(14); N4–Na1–N5, 89.93(15); N4–Na1–N6, 89.28(14); N5–Na1–N6, 174.85(15); C23–Zn1–C28, 114.28(18); C23–Zn1–C36, 117.38(19); C23–Zn1–N7, 97.57(18); C28–Zn1–C36, 119.81(18); C28–Zn1–N7, 99.22(17); C36–Zn1–N7, 102.47(14).

*via* a $2_1$ screw axis acting parallel to the crystallographic *c* direction. The chains pack into a layered structure. The layers lie parallel to the *ab* plane and each layer is composed only of $Na(py)_6$ or $ZntBu(py)_3$ units. These alternate in the *c* direction as shown in Fig. S14.†

Reports of characterised 4-metallated pyridine molecules are rare, particularly with respect to either zinc or the s-block. A series of structures have been published utilizing the heavier group 12 metal mercury although these have been prepared *via* mercury(II) acetate and the aryl boronic acid [28] or by preparing the Grignard reagent *via* metal–halogen exchange of 4-iodopyridine followed by metathesis with mercuric chloride.[29] Metal–halogen exchange is the principal route to metallated pyridines, although direct metallation with bimetallic alkali-metal complexes such as LiCKOR[30] or Caubere's base[31] is possible albeit metallation is predominantly directed α to the heteroatom.[32]

This reactivity with pyridine is in complete contrast to the reaction of **1** with toluene in that here, the parent tetrazincated ferrocenyl species exhibits simultaneous core and peripheral reactivity acting as a dual ferrocenyl/TMP base with retention of *t*butyl groups in **3** as opposed to acting as a *t*butyl base with retention of the TMP and ferrocenyl anions in **2**. This was further supported by the presence of TMP(H) and ferrocene in the $^1$H NMR spectrum of the filtrate.

As the yield of isolated recrystallized complex **3** was low (9%), the reaction was repeated in the less polar solvent hexane with pyridine slowly added until complete dissolution had been reached. Unfortunately, despite several attempts no solid product could be obtained with an orange oil separating from the solution instead. Attempts to recrystallize the product from toluene were also unsuccessful. After isolating the crystals from pyridine solution, the solvent was removed from the remaining solution under vacuum and analysed by $^1$H NMR spectroscopy but the presence of many overlapping resonances meant it was not possible to determine the presence of more **3** or any other metallation products. To gain more insight the reaction of **1**

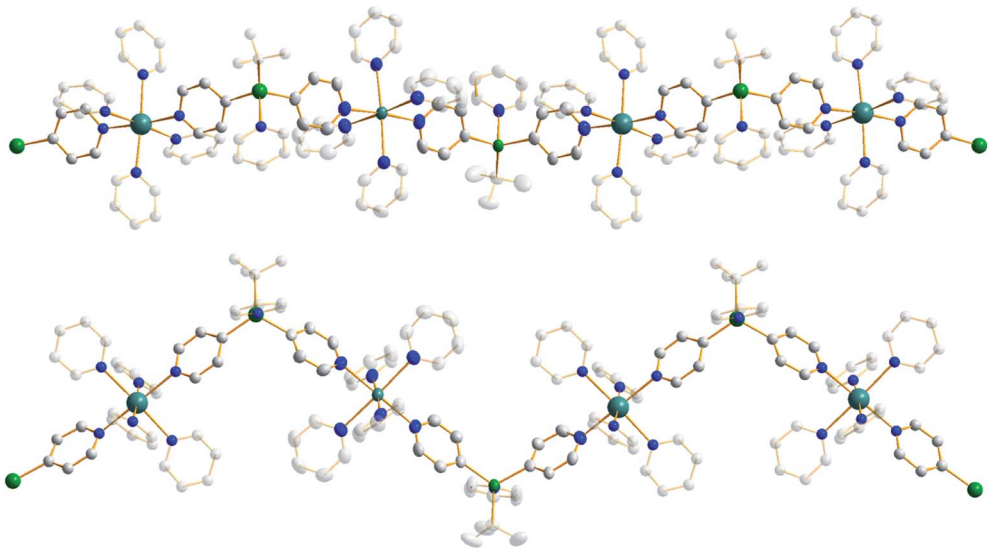

Fig. 7 Propagation of $\{[Na\cdot 4py][Zn(py^*)_2(tBu)\cdot py]\}_\infty$ (**3**) into a polymer shown from the side and above. Ellipsoids are shown at 50% probability, all hydrogen atoms have been removed and all *t*Bu carbon atoms and neutral donor pyridine ligands are highly transparent for clarity.

with pyridine was repeated *in situ* and then electrophilically quenched with iodine to assess the metallation outcome indirectly. After work-up, the organic products were studied *via* $^1$H NMR spectroscopy (Fig. 8), with the aromatic region revealing the presence of 4-iodopyridine (as expected) alongside 3-iodopyridine and some pyridine solvent. The ratio of 3-iodopyridine:4-iodopyridine was approximately 57 : 43 suggesting that 3-metallation is slightly more predominant while integration of these resonances *versus* an internal standard of hexamethylbenzene suggested that the total amount of pyridine metallation was under 20%. That the major 3-metallated product did not preferentially recrystallise perhaps suggests that it is a discrete molecule rather than a polymer (as in **3**) and thus is less inclined to precipitate from the highly polar pyridine solution. A literature search identified the report of a 3-zincated pyridyl compound exhibiting an eye-catching infinite stepladder arrangement made by reacting 4-methoxypyridine with the related mixed-metal base PMDETA·K(μ-TMP)(μ-Et)ZnEt. However, in this case the 4-position was blocked by a methoxy group which can be considered as a directing group towards the position *ortho* to itself (that is the 3-position).[33] The $Zn–C_{pyr}$ distance in this complex [2.062(4) Å] is almost identical to that of **3** [2.061(4) Å].

Interestingly, the peripheral reactivity towards toluene appears to be limited solely to the tetrazincated ferrocene complex **1**. Dizincated ferrocene complex **B** is inert to toluene as

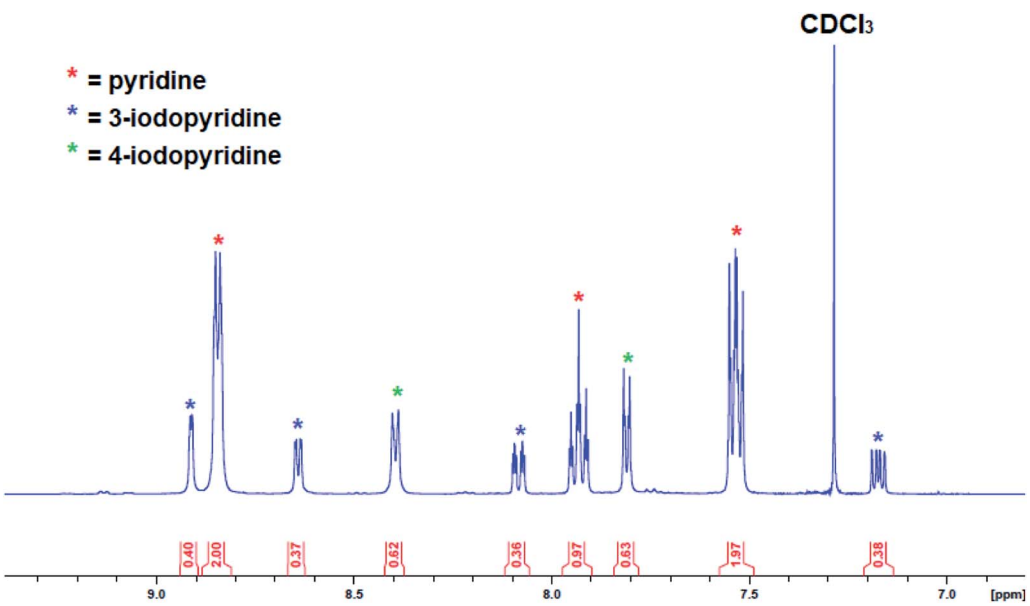


Fig. 8 Aromatic region of the $^1$H NMR spectrum (in $CDCl_3$) of work-up products after reaction of complex **1** with pyridine followed by an iodine quench.

 

demonstrated by the molecular structure of the recrystallised product upon refluxing in neat toluene, which is simply **B** with a toluene molecule of crystallisation trapped within the lattice (Fig. S15†). Likewise, a $^1$H NMR spectrum of complex **B** refluxed in pyridine showed no evidence of heterocycle metallation.

# Conclusions

Zinc alkyls and homometallic zinc compounds in general are exceptionally poor bases due primarily to insufficient Zn–C bond polarity, but here through the assistance of sodium TMP, a fourfold deprotonation of ferrocene is accomplished. While alkali-metal-mediated zincation (AMMZn) is well established, to our knowledge this is the only example where four C–H to C–Zn(R) transformations have been reported on a single molecule. A single crystal structure determination supported by DFT studies have elucidated a discrete open inverse crown arrangement where two $[Na(TMP)Zn(tBu)Na(TMP)Zn(tBu)]^{2+}$ cationic units trap a $\{(C_5H_3)_2Fe\}^{4-}$ tetraanion. Reactions of this polyzincated complex with toluene and pyridine result in different outcomes. The former produces two benzyl anions which replace two of the alkyl substituents in $[Na_4(TMP)_4Zn_4(tBu)_4\{(C_5H_3)_2Fe\}]$ to give $[Na_4(TMP)_4Zn_4(tBu)_2(CH_2Ph)_2\{(C_5H_3)_2Fe\}]$, which retains the gross inverse crown structure. In contrast, the latter produces $\{[Na\cdot 4py][Zn(py^*)_2(tBu)\cdot py]\}_\infty$, a zig–zag chain polymer possessing both neutral and deprotonated (at the 4-position) pyridine ligands. These initial studies suggest that $[Na_4(TMP)_4Zn_4(tBu)_4\{(C_5H_3)_2Fe\}]$ has broad reactivity scope since it can utilise both peripheral (*t*-butyl, TMP) and core (ferrocenyl) anions in its reactions. Since methodologies to convert C–Zn bonds to other C–X bonds are well known, such polyzincated molecules may provide access to novel compounds and materials in future work which are of interest to synthetic, macromolecular and supramolecular scientists amongst others.

# Experimental

### General experimental

All reactions and manipulations were conducted under a protective argon atmosphere using either standard Schlenk techniques or an MBraun glove box fitted with a gas purification and recirculation unit. Solvents were dried by heating to reflux over sodium benzophenone ketyl and then distilled under nitrogen prior to use. $tBu_2Zn$ was prepared according to literature procedures.[22] All other chemicals were obtained from commercial sources and used as received. Elemental analyses were performed at the University of Strathclyde Elemental Analysis Service.

### X-ray crystallography

Crystallographic data were collected on Bruker APEX2 or Oxford Diffraction instruments using synchrotron, Mo K$\alpha$ or Cu K$\alpha$ radiation ($\lambda$ = 0.6814, 0.71073 and 1.54184 Å respectively). Structures were solved using SHELXS-97 or OLEX2, while refinement was carried out on $F^2$ against all independent reflections by the full matrix least-squares method using the SHELXL-97 or SHELXL-2018/3 program or by the GaussNewton algorithm using OLEX2. All non-hydrogen atoms were refined using anisotropic displacement parameters. Selected crystallographic details and refinement details are provided in Table S4.† CCDC 1972641–1972644 contains the supplementary crystallographic data for this paper.

### Theoretical calculations

DFT calculations were performed using the Gaussian 03 (ref. 34) package using the B3LYP [35] density functional and the 6-311(d, p)[36] basis set. After each geometry optimization a frequency analysis was performed.

### NMR spectroscopy

NMR data for signal assignment and chemical exchange analysis were acquired on a three r.f. channel Bruker AVANCE II$^+$ NMR spectrometer equipped with a 14.1 T UltraShield™ superconducting magnet housing a 5 mm ∅ BBO-z-ATMA probehead, which was maintained at 298 K. The sample was solubilized in $C_6D_6$. Data were acquired and processed under Topspin 3.5 patch level 7 running on a Hewlett-Packard Z420 Workstation equipped with an Intel Xeon CPU E5-1620 v2 processor operating at 3.70 GHz under Windows 7 Professional edition.

**Acquisition of 2D [$^1$H, $^{13}$C] correlation NMR data.** 2D [$^1$H, $^{13}$C] correlation data were acquired as multiplicity-edit 2D [$^1$H, $^{13}$C] HSQC (Bruker pulse program hsqcedetgpsisp2.3), 2D [$^1$H, $^{13}$C] HMBC (Bruker pulse program hmqcetgpl3nd) and multiplicity-edited 2D [$^1$H, $^{13}$C] HSQC-TOCSY (Bruker pulse program hsqcdiedetgpsisp.1). NMR data were typically acquired into 4096 complex data points over an $\omega_2$ frequency width of 5411.255 Hz (9.017 ppm, aq = 378 ms) centred at $\delta^1$H = 4.00 ppm. The offset frequency of the indirectly detected dimension was set to $\delta^{13}$C = 70 ppm for HSQC and HSQC-TOCSY and to $\delta^{13}$C = 100 ppm for HMBC NMR data acquisitions with frequency widths equivalent to 165 ppm and 250 ppm respectively. Data were acquired at high resolution in the indirectly detected dimension with a total of 1024 and 2048 echo-antiecho $t_1$ increments for HSQC/HSQC-TOCSY and HMBC acquisitions respectively. Typically, acquisitions were performed with 25% non-uniform sampling in $\omega_1$ using 16 transients per $t_1$ increment.

**Acquisition of 2D [$^1$H, $^1$H] correlation NMR data.** 2D [$^1$H, $^1$H] NOESY/EXSY and supporting f1-PSYCHE-TOCSY [37] correlation data were acquired over $\omega_2$ and $\omega_1$ frequency widths equivalent to 9 ppm (5405 Hz) centred at $\delta^1$H = 4.00 ppm. Mixing times of 1 s and 70 ms respectively were used for the two types of data acquisitions. The data were acquired with 8 transients into 2048 data points for each of 512 State-TPPI and 2048 TPPI $t_1$ increments respectively.

All data assignments were carried out exclusively within the NMRFAM-SPARKY edition of the NMR data handling software package SPARKY.[38]

**Chemical exchange rates.** Chemical exchange rates were determined based on integration of the 1D $^1$H NMR spectrum of the CpH27, CpH27′, CpH28 and CpH28′ signals to give the ratio, major/minor, of the complex forms and through

integration of both cross-peaks and auto-correlation (diagonal) peaks in the relevant exchange cross-peak region of the 2D [$^1$H, $^1$H] NOESY/EXSY NMR data set with mixing time of 1 s. No account was taken for the leakage of the some of the magnetization into the form of nOe intensities. Calculation of the exchange rates was carried out based on a four-site exchange model using the standalone program EXSYCalc.[39] The estimates are based on one data set alone, which was available at the time of the study. A more rigorous and detailed analysis of this process, including estimates of activation and thermodynamic parameters is beyond the scope of this article for reasons of limited amounts of exchange-related data. For the same reason, a full investigation of the structure of the minor form of the complex has not been attempted in this work.

**[Na$_4$(TMP)$_4$Zn$_4$(*t*Bu)$_4$\{(C$_5$H$_3$)$_2$Fe\}] (1).** A Schlenk flask was charged with *t*Bu$_2$Zn (0.358 g, 2 mmol) that was dissolved in hexane (10 mL). In a separate Schlenk flask *n*BuNa (0.160 g, 2 mmol) was suspended in hexane (10 mL), and TMP(H) (0.34 mL, 2 mmol) was added *via* syringe, the resulting creamy white suspension being allowed to stir for an hour. Next the *t*Bu$_2$Zn solution was added *via* syringe followed by ferrocene (0.09 g, 0.5 mmol) *via* a solid addition tube. This mixture was stirred for 2 h, during which time the suspension changed from yellow to orange to red. The resulting red powder was collected *via* filtration, washed with hexane, and dried (0.464 g, 70%). A small crop of single crystals grew from the hexane filtrate at room temperature over 24 hours. Anal. calcd (%) for $C_{62}Fe_1H_{114}N_4Na_4Zn_4$: C, 56.20; H, 8.67; N, 4.23. Found: C, 56.24; H, 8.56; N, 4.32.

**[Na$_4$(TMP)$_4$Zn$_4$(*t*Bu)$_2$(CH$_2$Ph)$_2$\{(C$_5$H$_3$)$_2$Fe\}] (2).** Complex **1** was recrystallized from neat toluene yielding crystals of 2 (yield 0.249 g, 36%). Anal. calcd (%) for $C_{68}Fe_1H_{110}N_4Na_4Zn_4$: C, 58.63; H, 7.96; N, 4.02. Found: C, 58.10; H, 7.96; N, 3.95.

**[Na·4py][Zn(py*)$_2$(*t*Bu)·py] (3).** Complex **1** was dissolved in neat pyridine and cooled down, yielding crystals of 3 (yield 0.128 g, 9%). Despite repeated attempts no satisfactory elemental analyses could be obtained.

$^1$H NMR (400.13 MHz, $NC_5D_5$, 300 K): $\delta$ 0.51 [9H, s, *t*Bu], 8.24 [4H, d, $^3J$(H,H) = 4.8 Hz, −py β H], 8.59 [4H, d, $^3J$(H,H) = 4.80 Hz, −py α H]. $^{13}$C NMR (100.6 MHz, $NC_5D_5$, 300 K): $\delta$ 0.2 [*t*Bu], 0.7 [*t*Bu], 137.1 [−py β C], 145.5 [−py α C], metallated pyridine carbon could not be resolved.

**[TMEDA·Na(μ-TMP)Zn*t*Bu]$_2$(C$_5$H$_4$)$_2$Fe·C$_7$H$_8$ (4).** 1 mmol of [TMEDA·Na(μ-TMP)Zn*t*Bu]$_2$(C$_5$H$_4$)$_2$Fe was prepared *in situ* and was refluxed in toluene and cooled, yielding crystals of 4 (0.221 g, 20%).

## Conflicts of interest

There are no conflicts to declare.

## Acknowledgements

W. C. wishes to thank the Science and Technology Funding Council for access to Synchrotron Radiation Source at Daresbury Laboratory.

## References

1 (*a*) W. N. Setzer and P. v. R. Schleyer, *Adv. Organomet. Chem.*, 1985, **24**, 353–451; (*b*) V. H. Gessner, C. Däschlein and C. Strohmann, *Chem.–Eur. J.*, 2009, **15**, 3320–3334; (*c*) H. J. Reich, *Chem. Rev.*, 2013, **113**, 7130–7178; (*d*) E. Carl and D. Stalke, in *Lithium Compounds in Organic Synthesis*, ed. R. Luisi and V. Capriati, Wiley-VCH, Weinheim, 2014, pp. 1–32.

2 R. E. Mulvey and S. D. Robertson, *Angew. Chem., Int. Ed.*, 2013, **52**, 11470–11487.

3 (*a*) R. E. Mulvey, F. Mongin, M. Uchiyama and Y. Kondo, *Angew. Chem., Int. Ed.*, 2007, **46**, 3802–3824; (*b*) S. D. Robertson, M. Uzelac and R. E. Mulvey, *Chem. Rev.*, 2019, **119**, 8332–8405.

4 E. Hevia and R. E. Mulvey, *Angew. Chem., Int. Ed.*, 2011, **50**, 6448–6450.

5 R. Neufeld and D. Stalke, *Chem.–Eur. J.*, 2016, **22**, 12624–12626.

6 A. Castello-Mico and P. Knochel, *Synthesis*, 2018, **50**, 155–169.

7 B. Haag, M. Mosrin, H. Ila, V. Malakhov and P. Knochel, *Angew. Chem., Int. Ed.*, 2011, **50**, 9794–9824.

8 (*a*) M. Schlosser, J. H. Choi and S. Takagishi, *Tetrahedron*, 1990, **46**, 5633–5648; (*b*) E. Baston, R. Maggi, K. Friedrich and M. Schlosser, *Eur. J. Org. Chem.*, 2001, 3985–3989; (*c*) W. Clegg, S. H. Dale, A. M. Drummond, E. Hevia, G. W. Honeyman and R. E. Mulvey, *J. Am. Chem. Soc.*, 2006, **128**, 7434–7435; (*d*) E. Nagaradja, F. Chevallier, T. Roisnel, V. Dorcet, Y. S. Halauko, O. A. Ivashkevich, V. E. Matulis and F. Mongin, *Org. Biomol. Chem.*, 2014, **12**, 1475–1487; (*e*) M. Y. A. Messaoud, G. Bentabed-Ababsa, M. Hedidi, A. Derdour, F. Chevallier, Y. S. Halauko, O. A. Ivashkevich, V. E. Matulis, L. Picot, V. Thiery, T. Roisnel, V. Dorcet and F. Mongin, *Beilstein J. Org. Chem.*, 2015, **11**, 1475–1485; (*f*) M. Hedidi, W. Erb, F. Lassagne, Y. S. Halauko, O. A. Ivashkevich, V. E. Matulis, T. Roisnel, G. Bentabed-Ababsa and F. Mongin, *RSC Adv.*, 2016, **6**, 63185–63189.

9 (*a*) A. J. Martinez-Martinez, A. R. Kennedy, R. E. Mulvey and C. T. O'Hara, *Science*, 2014, **346**, 834–837; (*b*) A. J. Martinez-Martinez, S. Justice, B. J. Fleming, A. R. Kennedy, I. D. H. Oswald and C. T. O'Hara, *Sci. Adv.*, 2017, **3**, e1700832.

10 A. J. Martinez-Martinez, D. R. Armstrong, B. Conway, B. J. Fleming, J. Klett, A. R. Kennedy, R. E. Mulvey, S. D. Robertson and C. T. O'Hara, *Chem. Sci.*, 2014, **5**, 771–781.

11 (*a*) *Ferrocenes, Ligands, Materials and Biomolecules*, P. Štěpnička, Wiley, Chichester, 2008; (*b*) K. Heinze and H. Lang, *Organometallics*, 2013, **32**, 5623–5625; (*c*) D. Astruc, *Eur. J. Inorg. Chem.*, 2017, 6–29; (*d*) M. Patra and G. Gasser, *Nat. Rev. Chem.*, 2017, **1**, 0066.

12 W. Clegg, K. W. Henderson, A. R. Kennedy, R. E. Mulvey, C. T. O'Hara, R. B. Rowlings and D. M. Tooke, *Angew. Chem., Int. Ed.*, 2001, **40**, 3902–3905.

 

13 B. Jennewein, S. Kimpel, D. Thalheim and J. Klett, *Chem.–Eur. J.*, 2018, **24**, 7605–7609.
14 R. A. Benkeser, D. Goggin and G. Schroll, *J. Am. Chem. Soc.*, 1954, **76**, 4025–4026.
15 For other crystallographically characterized zincated ferrocenyl complexes see: (*a*) H. R. L. Barley, W. Clegg, S. H. Dale, E. Hevia, G. W. Honeyman, A. R. Kennedy and R. E. Mulvey, *Angew. Chem., Int. Ed.*, 2005, **44**, 6018–6021; (*b*) A. S. Perucha, J. Heilmann-Brohl, M. Bolte, H.-W. Lerner and M. Wagner, *Organometallics*, 2008, **28**, 6170–6177; (*c*) N. Seidel, K. Jacob, P. Zanello and M. Fontani, *J. Organomet. Chem.*, 2001, **620**, 243–248; (*d*) E. Hevia, A. R. Kennedy and M. D. McCall, *Dalton Trans.*, 2012, **41**, 98–103; (*e*) W. Clegg, B. Conway, P. Garcia-Alvarez, A. R. Kennedy, J. Klett, R. E. Mulvey and L. Russo, *Dalton Trans.*, 2010, **39**, 62–65.
16 (*a*) M. Uchiyama and C. Wang, *Top. Organomet. Chem.*, 2014, **47**, 159–202; (*b*) A. Hernan-Gomez, E. Herd, M. Uzelac, T. Cadenbach, A. R. Kennedy, I. Borilovic, G. Aromi and E. Hevia, *Organometallics*, 2015, **34**, 2614–2623; (*c*) A. Hernan-Gomez, S. A. Orr, M. Uzelac, A. R. Kennedy, S. Barroso, X. Jusseau, S. Lemaire, V. Farina and E. Hevia, *Angew. Chem., Int. Ed.*, 2018, **57**, 10630–10634; (*d*) B.-K. Tao, H. Yang, Y.-Z. Hua and M.-C. Wang, *Org. Biomol. Chem.*, 2019, **17**, 4301–4310; (*e*) G. Trott, J. A. Garden and C. K. Williams, *Chem. Sci.*, 2019, **10**, 4618–4627.
17 (*a*) S. Sase, M. Jaric, A. Metzger, V. Malakhov and P. Knochel, *J. Org. Chem.*, 2008, **73**, 7380–7382; (*b*) C. C. C. Johansson Seechurn, M. O. Kitching, T. J. Colacot and V. Snieckus, *Angew. Chem., Int. Ed.*, 2012, **51**, 5062–5085; (*c*) L. C. McCann, H. N. Hunter, J. A. C. Clyburne and M. G. Organ, *Angew. Chem., Int. Ed.*, 2012, **51**, 7024–7027; (*d*) D. Haas, J. M. Hammann, R. Greiner and P. Knochel, *ACS Catal.*, 2016, **6**, 1540–1552.
18 R. E. Mulvey, *Chem. Commun.*, 2001, 1049–1056.
19 W. Clegg, E. Crosbie, S. H. Dale-Black, E. Hevia, G. W. Honeyman, A. R. Kennedy, R. E. Mulvey, D. L. Ramsay and S. D. Robertson, *Organometallics*, 2015, **34**, 2580–2589.
20 D. R. Armstrong, W. Clegg, S. H. Dale, D. V. Graham, E. Hevia, L. M. Hogg, G. W. Honeyman, A. R. Kennedy and R. E. Mulvey, *Chem. Commun.*, 2007, 598–600.
21 (*a*) P. C. Andrikopoulos, D. R. Armstrong, A. R. Kennedy, R. E. Mulvey, C. T. O'Hara and R. B. Rowlings, *Eur. J. Inorg. Chem.*, 2003, 3354–3362; (*b*) A. R. Kennedy, J. Klett, R. E. Mulvey, S. Newton and D. S. Wright, *Chem. Commun.*, 2008, 308–310; (*c*) X.-H. Lu, M.-T. Ma, Y.-M. Yao, Y. Zhang and Q. Shen, *Inorg. Chem. Commun.*, 2010, **13**, 1566–1568; (*d*) A. R. Kennedy, R. E. Mulvey, C. T. O'Hara, G. M. Robertson and S. D. Robertson, *Angew. Chem., Int. Ed.*, 2011, **50**, 8375–8378.
22 P. C. Andrikopoulos, D. R. Armstrong, H. R. L. Barley, W. Clegg, S. H. Dale, E. Hevia, G. W. Honeyman, A. R. Kennedy and R. E. Mulvey, *J. Am. Chem. Soc.*, 2005, **127**, 6184–6185.
23 P. C. Andrikopoulos, D. R. Armstrong, W. Clegg, C. J. Gilfillan, E. Hevia, A. R. Kennedy, R. E. Mulvey, C. T. O'Hara, J. A. Parkinson and D. M. Tooke, *J. Am. Chem. Soc.*, 2004, **126**, 11612–11620.
24 (*a*) L. Lochmann, H. Jakabův and L. Brandsma, *Collect. Czech. Chem. Commun.*, 1993, **58**, 1445–1451; (*b*) I. A. Topol, G. J. Tawa, R. A. Caldwell, M. A. Eissenstat and S. K. Burt, *J. Phys. Chem. A*, 2000, **104**, 9619–9624.
25 (*a*) D. R. Armstrong, J. Garcia-Alvarez, D. V. Graham, G. W. Honeyman, E. Hevia, A. R. Kennedy and R. E. Mulvey, *Chem.–Eur. J.*, 2009, **15**, 3800–3807; (*b*) W. Clegg, B. Conway, E. Hevia, M. D. McCall, L. Russo and R. E. Mulvey, *J. Am. Chem. Soc.*, 2009, **131**, 2375–2384.
26 (*a*) M. G. Davidson, D. Garcia-Vivo, A. R. Kennedy, R. E. Mulvey and S. D. Robertson, *Chem.–Eur. J.*, 2011, **17**, 3364–3369; (*b*) D. R. Armstrong, M. G. Davidson, D. Garcia-Vivo, A. R. Kennedy, R. E. Mulvey and S. D. Robertson, *Inorg. Chem.*, 2013, **52**, 12023–12032.
27 (*a*) W. Clegg, G. C. Forbes, A. R. Kennedy, R. E. Mulvey and S. T. Liddle, *Chem. Commun.*, 2003, 406–407; (*b*) J. A. Garden, A. R. Kennedy, R. E. Mulvey and S. D. Robertson, *Dalton Trans.*, 2011, **40**, 11945–11954.
28 D. V. Partyka and T. G. Gray, *J. Organomet. Chem.*, 2009, **694**, 213–218.
29 T. Mocanu, C. I. Rat, C. Maxim, S. Shova, V. Tudor, C. Silvestru and M. Andruh, *CrystEngComm*, 2015, **17**, 5474–5487.
30 J. Verbeek, A. V. E. George, R. L. P. de Jong and L. Brandsma, *J. Chem. Soc., Chem. Commun.*, 1984, 257–258.
31 P. Gros, Y. Fort and P. Caubere, *J. Chem. Soc., Perkin Trans. 1*, 1997, 3597–3600.
32 For a review of pyridine metallation chemistry see M. Schlosser and F. Mongin, *Chem. Soc. Rev.*, 2007, **36**, 1161–1172.
33 B. Conway, D. V. Graham, E. Hevia, A. R. Kennedy, J. Klett and R. E. Mulvey, *Chem. Commun.*, 2008, 2638–2640.
34 M. J. Frisch, G. W. Trucks, H. B. Schlegel, G. E. Scuseria, M. A. Robb, J. R. Cheeseman, J. A. Montgomery Jr, T. Vreven, K. N. Kudin, J. C. Burant, J. M. Millam, S. S. Iyengar, V. Tomasi, B. Barone, B. Mennucci, M. Cossi, G. Scalmani, N. Rega, G. A. Petersson, H. Nakatsuji, M. Hada, M. Ehara, K. Toyota, R. Fukuda, J. Hasegawa, M. Ishida, T. Nakajima, Y. Honda, O. Kitao, H. Nakai, M. Klene, X. Li, J. E. Knox, H. P. Hratchian, J. B. Cross, V. Bakken, C. Adamo, J. Jaramillo, R. Gomperts, R. E. Stratmann, O. Yazyev, A. J. Austin, R. Cammi, C. Pomelli, J. W. Ochterski, P. Y. Ayala, K. Morokuma, G. A. Voth, P. Salvador, J. J. Dannenberg, V. G. Zakrzewski, S. Dapprich, A. D. Daniels, M. C. Strain, O. Farkas, D. K. Malick, A. D. Rabuck, K. Raghavachari, J. B. Foresman, J. V. Ortiz, Q. B. Cui, A. G. Baboul, S. Clifford, J. Cioslowski, B. B. Stefanov, G. Liu, A. Liashenko, P. Piskorz, I. Komaromi, R. L. Martin, D. J. Fox, T. Keith, M. A. Al-Laham, C. Y. Peng, A. Nanayakkara, M. Challacombe, P. M. W. Gill, B. Johnson, W. Chen, M. W. Wong, C. Gonzalez and

J. A. Pople, *Gaussian 03 (Revision C.02)*, Gaussian Inc., Wallingford, CT, 2004.

35 (*a*) W. Kohn, A. D. Becke and R. G. Parr, *J. Phys. Chem.*, 1996, **100**, 12974–12980; (*b*) A. D. Becke, *Phys. Rev. A*, 1988, **38**, 3098–3100.

36 (*a*) A. D. McLean and G. S. Chandler, *J. Chem. Phys.*, 1980, **72**, 5639–5648; (*b*) R. Krishnan, J. S. Binkley, R. Seeger and J. A. Pople, *J. Chem. Phys.*, 1980, **72**, 650–654.

37 M. Foroozandeh, R. W. Adams, M. Nilsson and G. A. Morris, *J. Am. Chem. Soc.*, 2014, **136**, 11867–11869.

38 W. Lee, M. Tonelli and J. L. Markley, *Bioinformatics*, 2015, **31**, 1325–1327.

39 J. C. Cobas and M. Martin-Pastor, *EXSYCalc, 1.0*, Mestrelab Research, Santiago de Compostela.

 